

# Electrohydrodynamic Jet Printing Driven by a Triboelectric Nanogenerator

Changsheng Wu, Halil Tetik, Jia Cheng, Wenbo Ding, Hengyu Guo, Xingtian Tao, Nanjia Zhou, Yunlong Zi, Zhiyi Wu, Huixuan Wu, Dong Lin,\* and Zhong Lin Wang\*

Electrohydrodynamic jet (e-jet) printing is a high-resolution printed electronics technique that uses an electric field to generate droplets. It has great application potential with the rapid development of flexible and wearable electronics. Triboelectric nanogenerators (TENG), which can convert mechanical motions into electricity, have found many high-voltage applications with unique merits of portability, controllability, safety, and cost-effectiveness. In this work, the application of a TENG is extended to printed electronics by employing it to drive e-jet printing. A rotary freestanding TENG is applied as the high-voltage power source for generating stable ink droplet ejection. The TENG-driven droplet generation and ejection process and printed features with varied operation parameters are investigated. Results reveal that the jetting frequency could be controlled by the TENG's operation frequency, and high-resolution printing with feature size smaller than nozzle size is achieved using the setup. Notably, TENG as the power source for e-jet printing supplies a limited amount of current, which leads to better safety for both equipment and personnel compared to conventional high-voltage power supplies. With the superiority of TENG in the sense of safety and cost, the work presents a promising solution for the next-generation of high-resolution printed electronics and broadens the scope of TENG application.

development of flexible and wearable electronics over the past decade. These methods, when used to fabricate electronics devices by depositing functional inks onto various substrates, are often referred to as printed electronics.<sup>[4–6]</sup> Compared to conventional fabrication methods such as photolithography, printed electronics has attractive features including simple fabrication process, applicability on flexible substrates, compatibility with large-area substrates, and low fabrication cost. Among the various methods, inkjet printing, aerosol jet printing,<sup>[7,8]</sup> and electrohydrodynamic jet (e-jet) printing,<sup>[9,10]</sup> which enable mask-free fabrication in an additive rather than subtractive manner, endow manufacturers with the additional capability of directly patterning ink materials, and thus are more efficient in material usage and device design. They have been widely used for the fabrication of thin-film transistors, radiofrequency identifications, displays, biomedical devices, etc.<sup>[11]</sup> Specifically, inkjet printing deposits

## 1. Introduction

Various printing methods, such as screen printing<sup>[1]</sup> and inkjet printing,<sup>[2,3]</sup> have attracted enormous interest during the rapid

ink droplets on demand by supplying pressure pulses in the fluid-filled chamber and the pulses are triggered via thermal vaporization, acoustic agitation, or piezoelectric actuation.<sup>[12]</sup> Aerosol jet printing uses ultrasonic atomization to generate ink

C. Wu, Dr. W. Ding, Dr. H. Guo, Dr. Z. Wu,  
Prof. Z. L. Wang  
School of Materials Science and Engineering  
Georgia Institute of Technology  
Atlanta, GA 30332, USA  
E-mail: zhong.wang@mse.gatech.edu

H. Tetik, Prof. D. Lin  
Department of Industrial and Manufacturing  
Systems Engineering  
Kansas State University  
Manhattan, KS 66506, USA  
E-mail: dongl@ksu.edu

Prof. J. Cheng  
State Key Laboratory of Tribology  
Department of Mechanical Engineering  
Tsinghua University  
Beijing 100084, China

 The ORCID identification number(s) for the author(s) of this article can be found under <https://doi.org/10.1002/adfm.201901102>.

DOI: 10.1002/adfm.201901102

X. Tao, Prof. H. Wu  
Department of Aerospace Engineering  
University of Kansas  
Lawrence, KS 66049, USA

Prof. N. Zhou  
School of Engineering  
Westlake University  
18 Shilongshan Road, Hangzhou, Zhejiang Province 310024, China

Prof. N. Zhou  
Institute of Advanced Technology  
Westlake Institute for Advanced Study  
18 Shilongshan Road, Hangzhou, Zhejiang Province 310024, China

Prof. Y. Zi  
Department of Mechanical and Automation Engineering  
The Chinese University of Hong Kong  
Shatin, N.T., Hong Kong SAR, China

Prof. Z. L. Wang  
Beijing Institute of Nanoenergy and Nanosystems  
Chinese Academy of Sciences  
National Center for Nanoscience and Technology (NCNST)  
Beijing 100083, China

droplets, which are transported by a carrier gas and collimated by a sheath gas before being jetted toward the substrate.<sup>[7]</sup> In e-jet printing, an electric field is applied between the deposition nozzle and the substrate and induces mobile ions in the ink to accumulate at the liquid surface. The liquid meniscus is deformed into a conical shape, or the so-called Taylor cone,<sup>[13]</sup> due to the Coulombic repulsion of ions, and a droplet is ejected toward the substrate once the stress from the charge repulsion at the cone apex exceeds the surface tension.<sup>[14]</sup> Therefore, e-jet printing is capable of producing ink droplets much smaller than the nozzle and has been regarded as a high-resolution printing technique. A sub-micrometer resolution (up to 700 nm) has been demonstrated using e-jet printing, while the resolution limits of inkjet printing and aerosol jet printing are tens of micrometers.<sup>[9]</sup> It also avoids the inherent clogging issue in inkjet printing and aerosol jet printing by achieving comparable resolution with a much larger nozzle.<sup>[15]</sup> E-jet printing has great potential in high-resolution electronics printing and has been successfully used to print various materials including conductive inks,<sup>[15,16]</sup> DNA,<sup>[17]</sup> quantum dots,<sup>[18]</sup> and small organic molecules.<sup>[19]</sup> However, conventional high-voltage (HV) power sources required for the process generally have high cost and pose major threats to substrates, surrounding instruments and operation personnel.

Meanwhile, triboelectric nanogenerator (TENG), which can convert mechanical motions into electricity based on the coupling effects of triboelectrification and electrostatic induction, has experienced dramatic development since its invention in 2012.<sup>[20–26]</sup> Its theoretical origin can be traced back to Maxwell's equations, which gives TENG unique output characteristics of high voltage and low current.<sup>[27,28]</sup> Therefore, TENG may serve as a novel alternative of conventional HV power sources with unprecedented portability and safety.<sup>[29]</sup> The high voltage output (1–10 kV) of TENG, possibly driven by biomechanical motions for emergent use or environmental motions and small electric motors for longer use, eliminates the requirement of sophisticated power converters and thus reduces the system complexity and cost. Compared to commercial direct current (DC) HV power supplies, the limited current and charge transfer per cycle from TENG also makes it better for the safety of personnel and instrument. The high voltage automatically decreases as the limited charges are transferred. Therefore, TENG has found many high-voltage-driven applications, such as nanoelectrospray ionization for mass spectrometry,<sup>[30]</sup> microplasma,<sup>[31,32]</sup> electron field emission,<sup>[33]</sup> air cleaning,<sup>[34]</sup> electrospinning,<sup>[35]</sup> and electrostatic actuation.<sup>[36]</sup> In the application for nanoelectrospray ionization, TENG offered unprecedented control over ion generation owing to the limited charge transfer per operation cycle and thus provided enhanced sensitivity at low sample concentrations.<sup>[30]</sup> In the case of electron field emission, the ZnO nanowires based emitting device survived the high voltage of TENG but not the conventional power source.<sup>[33]</sup> As for air cleaning, the filtering performance could be significantly enhanced with the voltage output of TENG which was driven by wasted mechanical energy, such as vibration or wind.<sup>[34]</sup> Therefore, TENG-based high voltage power sources have great application potential with the advantages of portability, controllability, and safety.

In this work, we managed to use TENG to drive the e-jet printing process. A rotary freestanding TENG (RF-TENG)<sup>[37,38]</sup> connected with a simple boost circuit<sup>[31]</sup> could supply an open-circuit DC voltage above 1 kV, which was adequate to induce continuous droplet formation and ejection from the printing nozzle. The droplet jetting process was recorded using a high-speed camera with a variable frame rate up to 37 350 fps, clearly showing the tunability of jetting frequency via the control of TENG operation frequency. Effects of nozzle moving speed and nozzle size on printed features at different TENG rotation speeds were studied as well. The TENG-driven e-jet printing setup was able to achieve feature sizes smaller than the nozzle diameters, with a minimum feature size of 135  $\mu\text{m}$  using a nozzle diameter of 160  $\mu\text{m}$  in our experiments without dedicated optimization of printing parameters. This performance is comparable to that using a commercial DC HV power source and the resolution is expected to be further improved by reducing the nozzle size and optimizing the nozzle-to-substrate distance. We also demonstrated its use for printing graphics, conductive interconnects, and touch sensors. The TENG was simply operated using a rotary motor and the cost of the TENG device and boost circuit is less than 100 USD, while a commercial DC HV power source usually costs more than 1000 USD. With the merits of controllability, high resolution, low cost, and safety, we believe this TENG-driven e-jet printing process can be an excellent alternative of conventional DC HV-driven process.

## 2. Results and Discussion

A schematic representation of our proposed TENG-drive e-jet printing process is illustrated in **Figure 1a**. A RF-TENG is connected to the printing nozzle and the substrate through a voltage boost circuit. The movement of the printing nozzle is controlled via a robotic arm and ink inside the syringe is held steady via pneumatic control. The RF-TENG consists of two parts, one stator and one rotator, with the detailed structures shown in Figure S1 in the Supporting Information. The stator is made of an acrylic sheet as the substrate, an aluminum foil layer as the electrodes, and a polytetrafluoroethylene (PTFE) film as one triboelectric layer. In the aluminum foil layer, two interdigitated radial arrays of electrodes, with each having 12 sectors connected at either the inner rim or the outer rim, are evenly distributed on the acrylic substrate and serve as the two electrodes of TENG. The rotator is made of an acrylic sheet with 12 evenly distributed nylon films hanging on it. The size of the nylon films is rationally chosen so that their free parts can cover about one electrode sector during rotation. The rotator is connected to the shaft of a rotating motor (Oriental Motor, BLFM230-A) through the center hole. The working mechanism of RF-TENG is presented in **Figure 1b**. The triboelectrification between the nylon film and the PTFE film induces positive charges on nylon and negative charges on PTFE. As the nylon sweeps across the PTFE film with the rotator, electrons will flow from one electrode to another due to electrostatic induction. The interdigitated electrode design ensures that continuous alternating current electricity can be generated as the rotator moves. A boost circuit consisting of variable boost

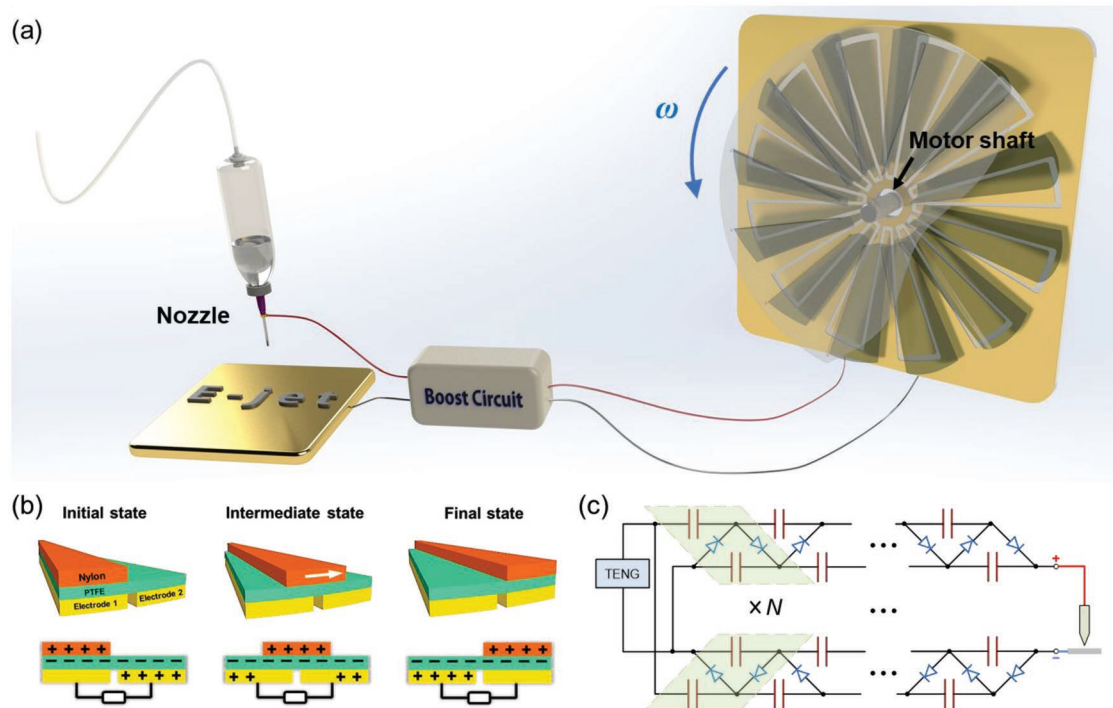


**Figure 1.** TENG-driven e-jet process. a) Schematic representation of the proposed process. b) Working mechanism of the sliding freestanding TENG. c) Equivalent electrical circuit model of the boost circuit.

units,<sup>[31]</sup> with its equivalent electrical circuit model shown in Figure 1c, is used to amplify the output voltage of the RF-TENG to achieve a steady, easily obtainable ink jetting process. Each boost unit consists of four capacitors of 4.7 nF and four high voltage diodes as highlighted in Figure 1c. Such a setup with five boost units achieved an open-circuit DC voltage above 1 kV as plotted in Figure S2 in the Supporting Information.

The nozzle-to-substrate distance is critical in the e-jet printing process. As shown in Figure 2a with a nozzle size of 340  $\mu\text{m}$ , when the distance was too small ( $\approx 0.5$  mm), the ink would deform and contact the substrate without droplet formation; when the distance was too large ( $\approx 2.5$  mm), the jetted droplets would breakup and thus a spray, rather than a series of drops, would be collected on the substrate, which is exactly the case for electro spraying.<sup>[39]</sup> Only with a proper distance ( $\approx 1$  mm), a stable stream of ink droplets could be ejected onto the substrate to achieve desirable printing resolution. To further validate the e-jet process driven by TENG, its droplet formation and ejection process was recorded using a high-speed camera (nac Image Technology, MEMRECAM HX-7), with one complete cycle shown as in Figure 2b,c for a motor rotation speed of 600 and 1000 RPM, respectively. The nozzle-to-substrate distance ( $\approx 5$  mm) was larger than that used in normal printing so that the camera lens could find a good focus position, and five boost units and a nozzle size of 600  $\mu\text{m}$  were used for the recording. During the e-jet process, the ink meniscus at the nozzle tip expands from spherical to conical shape and then contracts back to spherical shape periodically due to the electric field. A complete cycle can be divided into four phases, liquid accumulation, cone formation, droplet ejection, and relaxation.<sup>[14]</sup> During the liquid accumulation

phase (Figure 2b,c-i), ink accumulates at the nozzle tip and the meniscus is spherical with the surface tension as the dominant stress. Subsequently (Figure 2b,c-ii-iv), charges in the ink start to accumulate at the meniscus surface under the electric field and the resulted Maxwell stress from Coulombic repulsion transforms the meniscus into a conical shape. Once the Maxwell stress exceeds the surface tension (Figure 2b,c-viii), the radius of curvature at the cone apex reaches its minimum, and some charged ink liquid at the apex is ejected from the nozzle toward the collecting substrate and turns in to a droplet during the fall, resulting in a decrease in cone volume and charge amount. After the droplet ejection (Figure 2b,c-ix-x), the surface tension becomes dominant again and the meniscus retracts back to the spherical shape quickly, which is followed by the next cycle. This matches well with the droplet generation and ejection process reported in previous literature where a conventional DC HV is applied.<sup>[9,14]</sup>

To further study the effects of printing parameters on our TENG-driven e-jet process, we printed line and dot features at various nozzle moving speeds and nozzle sizes. For nozzle sizes of 160 and 210  $\mu\text{m}$ , a nozzle-to-substrate distance of 0.75 mm and three boost units were used; for 410 and 600  $\mu\text{m}$ , 1.5 mm and four boost units were used. The feature images are presented in Figures S3 and S4 in the Supporting Information for a motor rotation speed of 600 and 1000 RPM, respectively, and the results are summarized in Figure 3. Several observations can be made as follows. For one specific nozzle size, the width of the printed line feature decreased with the nozzle moving speed due to the reduced overlapping between successive droplets, until discrete dot features were printed. At a nozzle moving speed of 15  $\text{cm s}^{-1}$ , printed feature sizes smaller than the

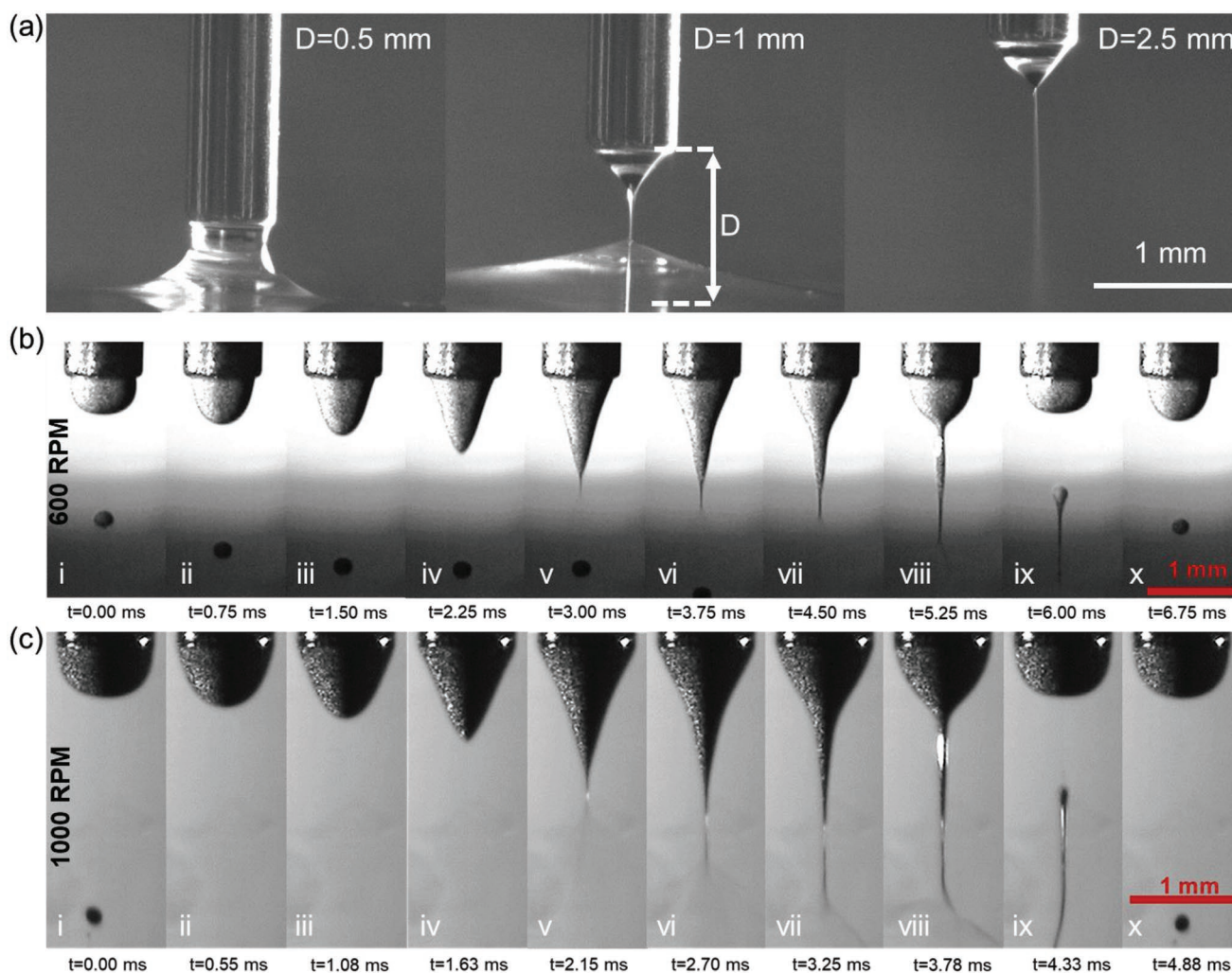


**Figure 2.** Photographs of the TENG-driven e-jet process. a) The significance of nozzle-to-substrate distance on achieving stable ink jetting. b,c) Droplet formation and ejection process recorded by high-speed camera with a motor rotation speed of b) 600 and c) 1000 RPM.

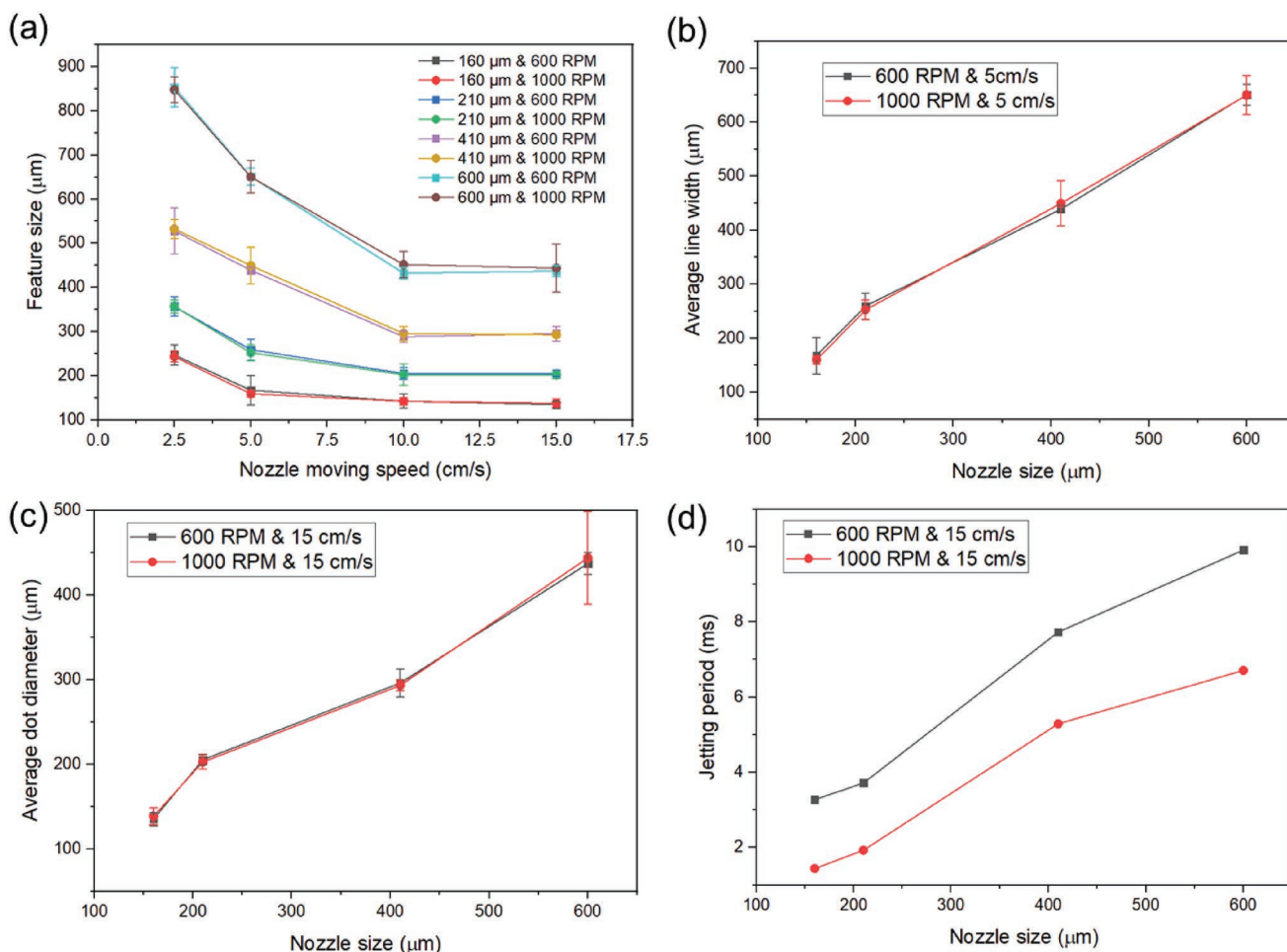
nozzle sizes were achieved for all, which clearly demonstrates the potential of high-resolution printing of our TENG-driven e-jet setup. The plots in Figure 3 also show a monotonically increasing correlation between the nozzle size and feature size as expected, regardless of the feature being line or dot.

Figure 3a–c shows that the change in motor rotation speed did not pose significant influence on the feature size in our experiments. However, one thing worth noting is that with all other parameters (ink, nozzle size, nozzle-to-substrate distance, nozzle moving speed, etc.) kept the same, the increase in motor rotation speed and thus TENG operation/voltage frequency decreased the jetting period, or increased the jetting frequency, which is supported by both the plot in Figure 3d and the images in Figure 2b,c. In previous literature about pulsed e-jet printing, such dependence of jetting frequency on the voltage frequency is generally attributed to the time interval between two successive pulses since one voltage pulse only ejects one droplet.<sup>[40–42]</sup> Two critical differences, however, existed in our setup. First, the TENG was operated in a continuous rotation mode and no time interval existed between two voltage cycles. Second, the motor rotation speed of 600 and 1000 RPM corresponds to a voltage

frequency of 120 and 200 Hz, i.e., a voltage cycle of 8.3 and 5 ms, respectively (see Note S1 in the Supporting Information). In such cases, for nozzle sizes of 160 and 210  $\mu\text{m}$ , more than one droplet was jetted within one TENG operation or voltage cycle. With a conventional power supply, a single voltage cycle with longer duration in the HV region gives more time for droplet ejection, and thus should have more droplets, which is contradictory to our experimental results. This is because of the unique characteristic of TENG, a power source with limited charge transfer. The output voltage of TENG when connected to a load is determined by the amount of charge transfer during the operation cycle and can be expressed as

$$V = -\frac{1}{C(z)} \times Q + V_{OC}(z) \quad (1)$$

where  $C$ ,  $z$ ,  $Q$ , and  $V_{OC}$  are the equivalent capacitance, displacement, charge transfer, and open-circuit voltage, respectively.<sup>[43]</sup> Meanwhile, it is the charge accumulation at the meniscus, rather the applied voltage, that directly triggers and is the root cause of the droplet ejection.<sup>[14]</sup> Therefore, it makes more sense



**Figure 3.** Effects of nozzle moving speed and nozzle size on printed features. a) Printed feature size with respect to different nozzle moving speed, nozzle size, and motor rotation speed. b) Printed line width at a constant nozzle moving speed of  $5 \text{ cm s}^{-1}$  with various nozzle sizes and motor rotation speeds. c) Printed dot diameter at a constant nozzle moving speed of  $15 \text{ cm s}^{-1}$  with various nozzle sizes and motor rotation speeds. d) Droplet jetting period with respect to different motor rotation speed.

to explain the results from the perspective of charge transfer. The maximum charge transfer per TENG operation cycle is independent of the operation frequency but the rate of charge transfer depends on the frequency. With the boost circuit, non-ideal capacitors and diodes would consume more charges when the operation cycle is longer, resulting in less amount that can be used for the jetting process. Consequently, the more rapidly the TENG rotates, the more quickly the charges accumulate at the liquid meniscus and thus the faster the droplets jet.

To better evaluate the performance of the TENG-driven e-jet printing process, a comparison study with the DC-driven process was conducted. With the same experimental setup, a DC voltage of 2000 V and a nozzle-to-substrate distance of 1 mm were applied to achieve stable ink jetting, whose printing results using different nozzles and moving speeds are presented in Figures S5 and S6 in the Supporting Information. Based on the comparison of Figures S3, S4 and S5 in the Supporting Information, the DC-driven jetting process produced all line features even at the highest moving speed of our robotic arm ( $15 \text{ cm s}^{-1}$ ), while the TENG-driven jetting process could generate dot features at smaller moving speeds ( $10 \text{ cm s}^{-1}$ ).

This indicates that a DC power supply, compared to our TENG, would give a much higher droplet jetting frequency. It could also be expected that by increasing the operation frequency of TENG, the printing results would become more similar with the DC-driven results. The motor rotation speed, i.e., TENG operation frequency, provides a facile method of controlling the droplet jetting frequency and the printed feature pattern (line or dot), especially in the case where nozzle moving speed is limited. A more quantitative comparison of the printed feature sizes (Figure 3a and Figure S6, Supporting Information) showed that the printed resolution using TENG is comparable with that using a DC power supply. Therefore, the TENG-driven e-jet printing process offers a promising alternative to conventional ones, not only with comparable resolution, but also with additional merits including low cost, extra safety, better feature controllability at low printing speeds, etc.

E-jet printing is commonly used for graphic arts,<sup>[9]</sup> so we first tried our TENG-driven setup for graphic printing. A pair of gears were printed as in Figure 4a. Printing of electrical components was also realized using our setup. Figure 4b shows two printed S-shaped conductive interconnects that could

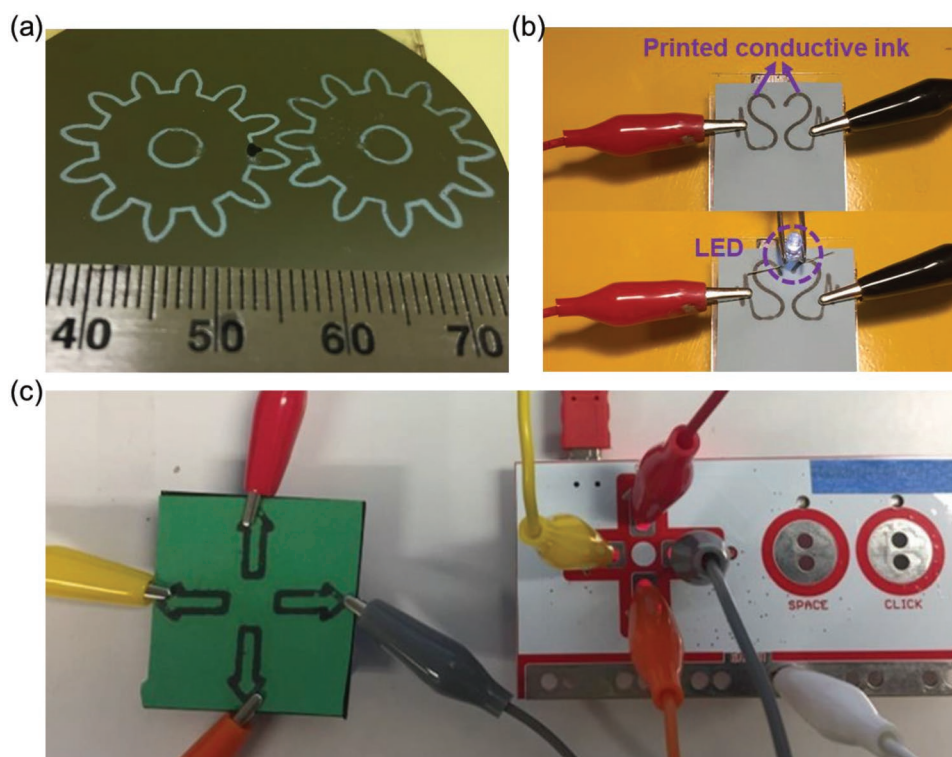


**Figure 4.** Demonstrations using the TENG-driven e-jet setup. a) Printed gear pattern. b) Printed electric interconnect. c) Printed sensor array for game control.

deliver the electric power from a battery to a light-emitting diode (LED) for lighting. In Figure 4c, we printed four conductive arrow patterns on a note paper. By integration with a MakeyMakey circuit, the patterns were successfully used as a sensing array and functioned as a directional keypad for controlling the gameplay of a virtual piano (Video S1, Supporting Information).

### 3. Conclusion

In this work, we explored the application of TENG in the field of printed electronics for the first time. A RF-TENG, together with a simple voltage boost circuit, was demonstrated to drive the e-jet printing process. The corresponding droplet formation and ejection process were examined using high-speed photography, and effects of various printing parameters, such as nozzle size and moving speed, nozzle-to-substrate distance, and motor rotation frequency, were studied. Results suggested that a configuration of smaller nozzle size, large nozzle moving speed, and optimal nozzle-to-substrate distance would yield smaller features. High-resolution printing with feature size smaller than nozzle size was achieved using our TENG-driven e-jet setup. Owing to the charge-dominating output characteristic of TENG, the droplet jetting frequency could be controlled by the TENG operation frequency. Several demonstrations, such as the printing of graphic art and the fabrication of conductive interconnects and touch sensors, were conducted to validate the potential of practical application

of the TENG-driven e-jet printing process. This works not only expands the application field of TENG, but also provides an alternative way of driving the high-resolution e-jet printing with unprecedented merits of safety, cost-effectiveness, and controllability.

### 4. Experimental Section

**TENG Fabrication:** The acrylic substrates (1/8 inch thick) of the stator and rotator were prepared using laser cutting according to the design in Figure S1 in the Supporting Information. Two aluminum films were pasted onto the inner and outer sections of the stator to function as the electrodes and then covered by a PTFE film (200  $\mu\text{m}$  thick) as one triboelectric material. The prepared nylon films (50  $\mu\text{m}$  thick) were partially inserted into and fixed on the slits of the rotator. All nylon films were bended in one direction so that they would not be twisted when sweeping across the stator clockwise. The rotator was fixed on the shaft of a rotating motor (Oriental Motor, BLFM230-A, 30 W and 0.6 kg) for motion control and the distance between the rotator and stator was adjusted so that the free part of a nylon film can cover about one electrode sector during rotation. The open-circuit voltage of the TENG was measured using a Keithley 6514 electrometer and a resistance-based voltage divider.

**E-jet Printing:** To perform the e-jet printing, the setup given in Figure 1a was prepared. The positive output of the boost circuit was attached to liquid dispensing nozzles (Brostown) having different diameters. The neutral output of the boost circuit was attached to a conductive silicon wafer (University Wafers 2270). The nozzle was attached to a syringe barrel (Nordson EFD) and the pressure inside the syringe barrel was controlled with a pneumatic dispenser (Nordson EFD, Ultimus III). A charge-coupled device (CCD) camera (Sentech STC, MB33USB) was used to observe the nozzle tip and meniscus formation.

The printing head, which consists of the dispensing nozzle, syringe barrel, and pneumatic dispenser, was placed on the end effector of a customized 3D printer (Geeetech-Rostock 301) and its motion as well as the moving speed was controlled by prepared g-codes. For a typical e-jet printing job, first, the vacuum level inside the printing head was adjusted so that a spherical meniscus could be observed at the nozzle tip without ink dropping. Following that, the printing head was moved to the home position at a distance of 150 mm from the substrate. In this position, due to the high distance between the substrate and nozzle tip, jetting would not start even if the TENG device was in operation. Afterward, the TENG device was started and the printing head was lowered to adjust the distance between the substrate and nozzle tip ( $\approx 0.5$ – $3$  mm). Once the printing head moved to the suitable position and jetting was observed through the CCD camera, the printing job was immediately started using the previously prepared g-codes. Except the Pac-Man patterns which used an aqueous carbon nanotube ink (Chasm Advanced Materials, AC100), all other printing jobs were completed with an Ag nanoparticles ink (Genes Ink, Smart Ink S-CS01130).

**Gameplay Demonstration:** For this demonstration, a commercial off-the-shelf electronic board from MakeyMakey was used, which could transform a variety of common objects into a user input device. It had the functions of arrow keys and space button from the keyboard and left click function from the mouse. In the experiment, the e-jet printed four arrow patterns on a piece of note paper using an aqueous carbon nanotube ink. These patterns were connected to the ports for arrow keys on the MakeyMakey board and grounded the board with one hand of the user using the white alligator clip, as shown in Figure 4c. As the user touched the printed patterns using the other hand, corresponding activation signals for the arrow keys were sent to the PC. As it can be seen in Video S1 in the Supporting Information, the user was able to play a virtual piano with the e-jet printed sensing array.

## Supporting Information

Supporting Information is available from the Wiley Online Library or from the author.

## Acknowledgements

C.W., H.T., and J.C. contributed equally to this work. Research was supported by the Hightower Chair foundation. D.L. thanks the support from the National Science Foundation under Award No. OIA-1656006 and matching support from the State of Kansas through the Kansas Board of Regents and the support from Johnson Cancer Center.

## Conflict of Interest

The authors declare no conflict of interest.

## Keywords

electrohydrodynamic jet printing, high voltage power sources, printed electronics, triboelectric nanogenerator

Received: February 3, 2019

Revised: March 7, 2019

Published online:

[1] F. C. Krebs, M. Jørgensen, K. Norrman, O. Hagemann, J. Alstrup, T. D. Nielsen, J. Fyenbo, K. Larsen, J. Kristensen, *Sol. Energy Mater. Sol. Cells* **2009**, *93*, 422.

- [2] H. Sirringhaus, T. Kawase, R. H. Friend, T. Shimoda, M. Inbasekaran, W. Wu, E. P. Woo, *Science* **2000**, *290*, 2123.
- [3] M. Singh, H. M. Haverinen, P. Dhagat, G. E. Jabbour, *Adv. Mater.* **2010**, *22*, 673.
- [4] J. Perelaer, P. J. Smith, D. Mager, D. Soltman, S. K. Volkman, V. Subramanian, J. G. Korvink, U. S. Schubert, *J. Mater. Chem.* **2010**, *20*, 8446.
- [5] M. Berggren, D. Nilsson, N. D. Robinson, *Nat. Mater.* **2007**, *6*, 3.
- [6] W. Wu, *Nanoscale* **2017**, *9*, 7342.
- [7] B. S. Ethan, *Flexible and Printed Electron.* **2018**, *3*, 035002.
- [8] C. Yung-Hang, W. Kan, W. Changsheng, C. Yiwen, Z. Chuck, W. Ben, *Smart Mater. Struct.* **2015**, *24*, 065008.
- [9] J.-U. Park, M. Hardy, S. J. Kang, K. Barton, K. Adair, D. k. Mukhopadhyay, C. Y. Lee, M. S. Strano, A. G. Alleyne, J. G. Georgiadis, P. M. Ferreira, J. A. Rogers, *Nat. Mater.* **2007**, *6*, 782.
- [10] C. Wu, B. Wang, C. Zhang, R. A. Wysk, Y.-W. Chen, *Crit. Rev. Biotechnol.* **2017**, *37*, 333.
- [11] R. Parashkov, E. Becker, T. Riedl, H. Johannes, W. Kowalsky, *Proc. IEEE* **2005**, *93*, 1321.
- [12] R. Sudipta, *J. Phys. D: Appl. Phys.* **2007**, *40*, R413.
- [13] I. Taylor Geoffrey, *Proc. R. Soc. London, Ser. A* **1964**, *280*, 383.
- [14] I. Marginean, L. Parvin, L. Heffernan, A. Vertes, *Anal. Chem.* **2004**, *76*, 4202.
- [15] K. Wang, M. D. Paine, J. P. W. Stark, *J. Appl. Phys.* **2009**, *106*, 024907.
- [16] L. Dae-Young, L. Jae-Chang, S. Yun-Soo, P. Sung-Eun, U. Y. Tae, K. Yong-Jun, H. Jung-ho, *J. Phys.: Conf. Ser.* **2008**, *142*, 012039.
- [17] J.-U. Park, J. H. Lee, U. Paik, Y. Lu, J. A. Rogers, *Nano Lett.* **2008**, *8*, 4210.
- [18] B. H. Kim, M. S. Onses, J. B. Lim, S. Nam, N. Oh, H. Kim, K. J. Yu, J. W. Lee, J.-H. Kim, S.-K. Kang, C. H. Lee, J. Lee, J. H. Shin, N. H. Kim, C. Leal, M. Shim, J. A. Rogers, *Nano Lett.* **2015**, *15*, 969.
- [19] K. Kim, G. Kim, B. R. Lee, S. Ji, S.-Y. Kim, B. W. An, M. H. Song, J.-U. Park, *Nanoscale* **2015**, *7*, 13410.
- [20] F.-R. Fan, Z.-Q. Tian, Z. Lin Wang, *Nano Energy* **2012**, *1*, 328.
- [21] Z. L. Wang, *Faraday Discuss.* **2014**, *176*, 447.
- [22] A. C. Wang, C. Wu, D. Pisignano, Z. L. Wang, L. Persano, *J. Appl. Polym. Sci.* **2018**, *135*, 45674.
- [23] J. Wang, C. Wu, Y. Dai, Z. Zhao, A. Wang, T. Zhang, Z. L. Wang, *Nat. Commun.* **2017**, *8*, 88.
- [24] X. Pu, H. Guo, J. Chen, X. Wang, Y. Xi, C. Hu, Z. L. Wang, *Sci. Adv.* **2017**, *3*, e1700694.
- [25] H. Guo, X. Pu, J. Chen, Y. Meng, M.-H. Yeh, G. Liu, Q. Tang, B. Chen, D. Liu, S. Qi, C. Wu, C. Hu, J. Wang, Z. L. Wang, *Sci. Rob.* **2018**, *3*, eaat2516.
- [26] G. Liu, J. Chen, Q. Tang, L. Feng, H. Yang, J. Li, Y. Xi, X. Wang, C. Hu, *Adv. Energy Mater.* **2018**, *8*, 1703086.
- [27] Z. L. Wang, *Mater. Today* **2017**, *20*, 74.
- [28] Z. L. Wang, T. Jiang, L. Xu, *Nano Energy* **2017**, *39*, 9.
- [29] C. Wu, A. C. Wang, W. Ding, H. Guo, Z. L. Wang, *Adv. Energy Mater.* **2019**, *9*, 1802906.
- [30] A. Li, Y. Zi, H. Guo, Z. L. Wang, F. M. Fernández, *Nat. Nanotechnol.* **2017**, *12*, 481.
- [31] J. Cheng, W. Ding, Y. Zi, Y. Lu, L. Ji, F. Liu, C. Wu, Z. L. Wang, *Nat. Commun.* **2018**, *9*, 3733.
- [32] F. Liu, Y. Liu, Y. Lu, Z. Wang, Y. Shi, L. Ji, J. Cheng, *Nano Energy* **2019**, *56*, 482.
- [33] Y. Zi, C. Wu, W. Ding, X. Wang, Y. Dai, J. Cheng, J. Wang, Z. Wang, Z. L. Wang, *Adv. Funct. Mater.* **2018**, *28*, 1800610.
- [34] S. Chen, C. Gao, W. Tang, H. Zhu, Y. Han, Q. Jiang, T. Li, X. Cao, Z. Wang, *Nano Energy* **2015**, *14*, 217.
- [35] C. Li, Y. Yin, B. Wang, T. Zhou, J. Wang, J. Luo, W. Tang, R. Cao, Z. Yuan, N. Li, X. Du, C. Wang, S. Zhao, Y. Liu, Z. L. Wang, *ACS Nano* **2017**, *11*, 10439.

- [36] X. Chen, T. Jiang, Y. Yao, L. Xu, Z. Zhao, Z. L. Wang, *Adv. Funct. Mater.* **2016**, 26, 4906.
- [37] G. Zhu, J. Chen, T. Zhang, Q. Jing, Z. L. Wang, *Nat. Commun.* **2014**, 5, 3426.
- [38] T. Jiang, X. Chen, C. B. Han, W. Tang, Z. L. Wang, *Adv. Funct. Mater.* **2015**, 25, 2928.
- [39] C. H. Chen, D. A. Saville, I. A. Aksay, *Appl. Phys. Lett.* **2006**, 89, 124103.
- [40] Y. Xin, X. Zhenhua, *J. Micromech. Microeng.* **2018**, 28, 095008.
- [41] S. Mishra, K. L. Barton, A. G. Alleyne, P. M. Ferreira, J. A. Rogers, *J. Micromech. Microeng.* **2010**, 20, 095026.
- [42] J. Yang, B. Cho, J. Chung, *J. Mech. Sci. Technol.* **2018**, 32, 3775.
- [43] S. Niu, Y. Liu, S. Wang, L. Lin, Y. S. Zhou, Y. Hu, Z. L. Wang, *Adv. Mater.* **2013**, 25, 6184.